engineering proceedings

MDPI

Proceeding Paper

Reduction in the Driving Force in Bottom-Driven Scissor Lifts †

Volodymyr Gurskyi *, Nadiia Maherus and Volodymyr Borovets

Department of Robotics and Integrated Mechanical Engineering Technologies, Lviv Polytechnic National University, 79013 Lviv, Ukraine; nadiia.i.maherus@lpnu.ua (N.M.); volodymyr.m.borovets@lpnu.ua (V.B.)

* Correspondence: volodymyr.m.hurskyi@lpnu.ua

† Presented at the 3rd International Electronic Conference on Machines and Applications, 12–14 May 2026; Available online: https://sciforum.net/event/IECMA2026.

Abstract

Scissor lifts are versatile lifting mechanisms that must satisfy stringent safety and reliability requirements. Therefore, accurate determination of their force and kinematic parameters is essential. An analytical approach for the design calculation of a bottom-driven scissor lift was developed. The proposed approach incorporates extension and compression springs to reduce the required driving force in the lowest platform position and improve the energy efficiency of the mechanism. A force analysis model of the scissor lift was developed, and the support reactions and the required driving force were determined as functions of the platform lifting height. Based on the kinematic analysis, the extreme linear and angular displacements of the scissor mechanism arms were determined. The functional dependences of the upper and lower spring deformations on the inclination angle of the scissor arms were established, characterizing the operating behavior of the load compensation system. The results demonstrate that the proposed spring compensation system reduced the required driving force by 26.5% and the internal forces in the scissor mechanism by 19.8–39.6% compared with the configuration without spring compensation. The developed analytical approach enables the determination of the force and energy characteristics of a bottom-driven scissor lift and the selection of reasonable spring parameters to reduce drive energy consumption.

Keywords: driving force; scissor lift; pantograph mechanism; ball screw; force analysis; kinematic characteristics; spring

1. Introduction

Pantograph mechanisms are the most widely used parallel kinematic mechanisms. Their advantages include single-drive architecture, high dynamic performance, and high positioning accuracy. The application of pantograph mechanisms is increasingly expanding in mobile robotic platforms and scissor lifts [1,2]. Various drive configurations were proposed for scissor lift platforms to provide vertical motion [3]. The simplest configuration employs a bottom-mounted horizontal linear actuator [4]. In such systems, hydraulic actuators [5] and screw–nut mechanisms [6,7] are the most commonly used drive solutions. However, this configuration requires the maximum driving force when the platform is in its lowest position, while the required force decreases with increasing lifting height. Another limitation of this design is that the platform cannot be fully folded. A roller-based drive configuration capable of fully folding the platform was presented in [8]. A key characteristic of scissor lifts is that the driving force varies nonlinearly with both the platform lifting height and the geometric configuration of its application points.

Check for updates

Academic Editor: Marco Ceccarelli

Published: 7 August 2026

Copyright: © 2026 by the authors. Licensee MDPI, Basel, Switzerland. This article is an open access article distributed under the terms and conditions of the Creative Commons Attribution (CC BY) license.

Nevertheless, scissor lift mechanisms exhibit complex dynamic behavior and require sophisticated analytical and numerical approaches. Previous studies have primarily focused on reducing structural weight [9], ensuring compliance with safety requirements, and improving drive systems. However, analytical approaches aimed at reducing the driving force through passive load compensation using elastic elements have received considerably less attention. Their use has been shown to improve both the static and dynamic performance of scissor lift mechanisms, as demonstrated in previous studies [1,2]. However, determining the reasonable parameters and configuration of elastic elements requires a comprehensive approach combining parameter synthesis and dynamic analysis.

Consequently, the analysis and modeling of scissor lift mechanisms incorporating spring-assisted drive compensation remain important research challenges.

2. Methods

General methods of static and kinematic analysis were employed in the study. A calculation scheme was formulated, and analytical expressions were derived along with graphical representations of the support reactions, driving force, and additional restoring forces as functions of the arm inclination angle. The stiffness coefficients of the elastic elements were selected based on preliminary design considerations, providing an initial basis for the analytical investigation. Rolling friction in the joints was neglected during the force analysis. The required motor power for the ball screw drive was determined by taking into account the known efficiency values of the transmission components.

3. Force Analysis of the Scissor Lift Mechanism

The scissor lift mechanism (Figure 1) consists of two pairs of arms, denoted I and II. To reduce the load on the lifting drive when the platform is in its lowest position, extension springs (1) and compression springs (2) are incorporated into the mechanism. The upper extension springs (1) operate throughout the entire range of arm motion, whereas the compression springs (2) are active only within a limited range of arm motion.

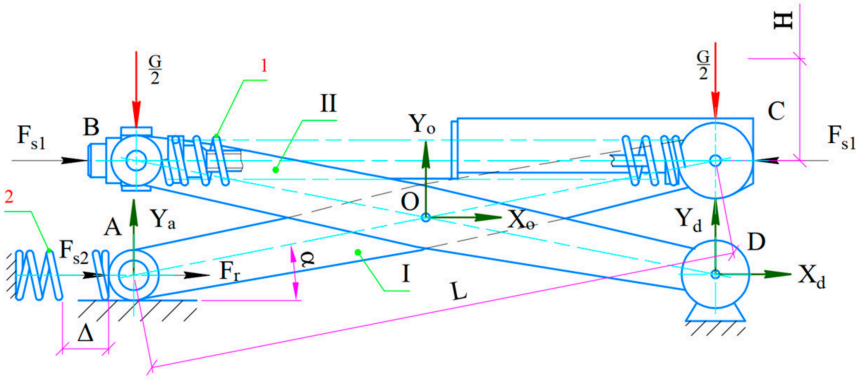


Figure 1. Force analysis diagram of the scissor lift.

The force analysis is based on the diagram shown in Figure 1. In this model, G is the total weight, G = 1.5 kN; F_r is the driving force; F_{s1}, F_{s2} are the restoring forces generated by the springs; X_i, Y_i are the reactions at the supports and the pin joint; α is the arm inclination angle; H is the lifting height, H = 400 mm; L is the arm length, L = 720 mm; Δ is the lower spring compression.

The force analysis involves six unknown quantities, namely X_o, Y_o, X_d, Y_d, Y_a and F_r. Accordingly, six independent equilibrium equations are required.

Based on the force diagram, the following equilibrium equations are obtained.

https://doi.org/10.3390/engproc2026145010

For arm I:

$$\begin{gathered}\sum_i F_{ix} = 0:\ X_o + F_r + F_{s2} - F_{s1} = 0;\\ \sum_i F_{iy} = 0:\ Y_a + Y_o - \tfrac{G}{2} = 0;\\ \sum M(F_i)_A = 0:\ \tfrac{G}{2}L\cos\alpha - Y_o\tfrac{L}{2}\cos\alpha + X_o\tfrac{L}{2}\sin\alpha - F_{s1}L\sin\alpha = 0.\end{gathered} \quad (1)$$

For arm II (assuming symmetry of the reactions at the pin joint):

$$\begin{gathered}\sum_i F_{ix} = 0:\ -X_o + X_d + F_{s1} = 0;\\ \sum_i F_{iy} = 0:\ -Y_o + Y_d - \tfrac{G}{2} = 0;\\ \sum M(F_i)_D = 0:\ -\tfrac{G}{2}L\cos\alpha - X_o\tfrac{L}{2}\sin\alpha - Y_o\tfrac{L}{2}\cos\alpha + F_{s1}L\sin\alpha = 0.\end{gathered} \quad (2)$$

Solving the systems of equations (Equation (1)) and (Equation (2)) yields the following unknown quantities:

$$\begin{bmatrix} X_o\\ Y_o\\ Y_a\\ X_d\\ Y_d\\ F_r \end{bmatrix} = \begin{bmatrix} 2F_{s1} - G\cot\alpha\\ 0\\ \frac{G}{2}\\ F_{s1} - G\cot\alpha\\ \frac{G}{2}\\ G\cot\alpha - F_{s1} - F_{s2} \end{bmatrix}. \quad (3)$$

To verify the obtained solution, an additional equilibrium equation was formulated for arm I using the analytical expressions given in Equation (3):

$$\sum M(F_i)_O = 0:\ \frac{G}{2}\frac{L}{2}\cos\alpha + Y_a\frac{L}{2}\cos\alpha - (F_{s2} + F_r)\frac{L}{2}\sin\alpha - F_{s1}\frac{L}{2}\sin\alpha = 0.$$

4. Kinematic Analysis of the Scissor Lift Mechanism

The distance between the joints in the upper and lower positions (Figure 2) is defined as $h_{max} = L\sin(\alpha_{max})$ and $h_{min} = L\sin(\alpha_{min})$, respectively. The lifting height of the platform is $H = h_{max} - h_{min} = L(\sin(\alpha_{max}) - \sin(\alpha_{min}))$. For the considered scissor lift mechanism, the minimum and maximum distances between the joints are $h_{min} = 200$ mm and $h_{max} = H + h_{min} = 600$ mm, respectively. Therefore, the maximum and minimum rotation angles of arm I are determined as follows:

$$\alpha_{max} = \arcsin\left(\frac{h_{max}}{L}\right) = \arcsin\left(\frac{0.6}{0.72}\right) = 56.4^\circ;$$

$$\alpha_{min} = \arcsin\left(\frac{h_{min}}{L}\right) = \arcsin\left(\frac{0.2}{0.72}\right) = 16.1^\circ.$$

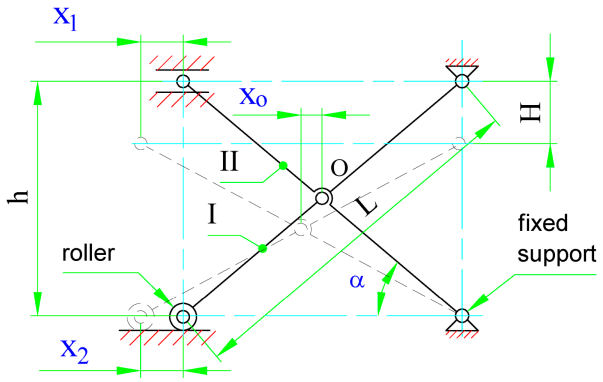


Figure 2. Joint displacement diagram.

The horizontal displacement of the upper joint is determined based on the rotational motion of arm II:

$$x_1 = L(\cos(\alpha_{min}) - \cos(\alpha_{max})) = 720(\cos 16.1^\circ - \cos 56.4^\circ) = 293.3 \text{ mm}.$$

Arm I performs general plane motion, which can be decomposed into translational and rotational motions. The linear displacement of the lower roller is given by $x_2 = x_O + \frac{L}{2}(\cos(\alpha_{min}) - \cos(\alpha_{max}))$.

Since the central pin joint is located at the midpoint of the arms (point O), at a distance of $\frac{L}{2}$, it follows that $x_O = 0.5x_1$, and therefore $x_2 = x_1$.

For the analyzed scissor lift mechanism, the platform vertical displacement is $H = 400$ mm, whereas the horizontal displacement of the lower roller is $x_1 = 293.3$ mm. The ratio of the platform vertical displacement to the horizontal displacement of the lower roller is given by

$$\frac{H}{x_2} = \frac{\sin(\alpha_{max}) - \sin(\alpha_{min})}{\cos(\alpha_{min}) - \cos(\alpha_{max})} = \frac{\sin(56.4^\circ) - \sin(16.1^\circ)}{\cos(16.1^\circ) - \cos(56.4^\circ)} = 1.36. \quad (4)$$

Accordingly, the average platform lifting speed is governed by this ratio. Therefore, for a specified platform lifting speed, the corresponding lower roller speed can be determined.

5. Scissor Lift Mechanism Operation Analysis

The upper springs are initially unstretched when the arms are in the upper position. During platform lowering, the springs extend and reach their maximum elongation when the platform reaches its lowest position. Therefore, the restoring force F_{s1} reduces the required driving force F_r throughout the entire motion range of the platform.

In contrast, the lower springs operate in compression and have a limited operating range. Specifically, they are active only in the lower position of the platform, when the arm inclination angle is less than 25°:

$$\Delta(\alpha) = \begin{Bmatrix} k \cdot \alpha + b, & if\ \alpha < 25^\circ, \\ 0 & otherwise. \end{Bmatrix} \quad (5)$$

where $k = \frac{x_2(25deg)}{\alpha_{min} - 25deg}$ and $b = -\frac{x_2(25deg) \cdot 25deg}{\alpha_{min} - 25deg}$.

Accordingly, the restoring force F_{s2} also reaches its maximum value in the lowest position, where the lower springs are maximally compressed. The extension of the upper springs and the compression of the lower springs as functions of the arm inclination angle are shown in Figure 3.

The upper extension springs have dimensions $5.5 \times 45 \times 530$ mm, whereas the lower compression springs have dimensions $4 \times 32 \times 120$ mm. These dimensions correspond to spring stiffness coefficients of $c_1 = 3.5$ N/mm and $c_2 = 9.2$ N/mm, respectively.

Based on the operating conditions of the springs, the restoring forces F_{s1} and F_{s2} are expressed as follows:

$$\begin{aligned} F_{s1}(\alpha) &= c_1 \cdot x_1(\alpha_{max}) - c_1 \cdot x_1(\alpha); \\ F_{s2}(\alpha) &= c_2 \cdot \Delta(\alpha). \end{aligned} \quad (6)$$

The operating characteristics of the springs are illustrated in Figure 4. In the lower position of the platform, the upper spring reaches its maximum extension, and consequently, the restoring force F_{s1} attains its maximum value. As the platform is raised, the spring gradually returns to its unstretched state, causing F_{s1} to decrease to zero in the upper position. The lower spring reaches its maximum compression in the lower position. As the platform is raised and the arm inclination angle increases to $\alpha = 25^\circ$, the spring gradually

https://doi.org/10.3390/engproc2026145010

returns to its free length. Consequently, its contribution to the loading of the mechanism arms is limited. The upper spring provides the primary contribution to the static force characteristics, as it operates throughout the entire platform lifting range. The lower spring mainly influences the deceleration of the platform during lowering. These effects will be investigated in the dynamic analysis of the scissor lift.

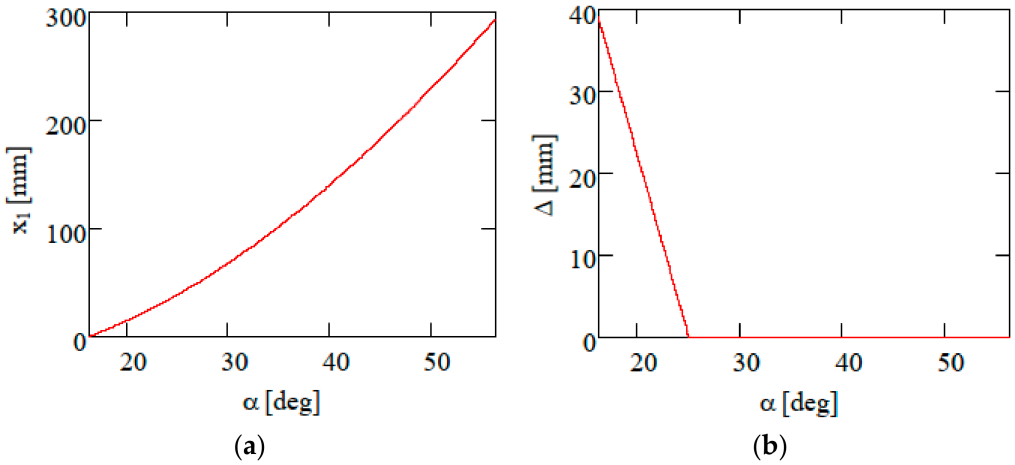


Figure 3. Dependences of spring deformations on the arm inclination angle: (**a**) extension of the upper spring; (**b**) compression of the lower spring.

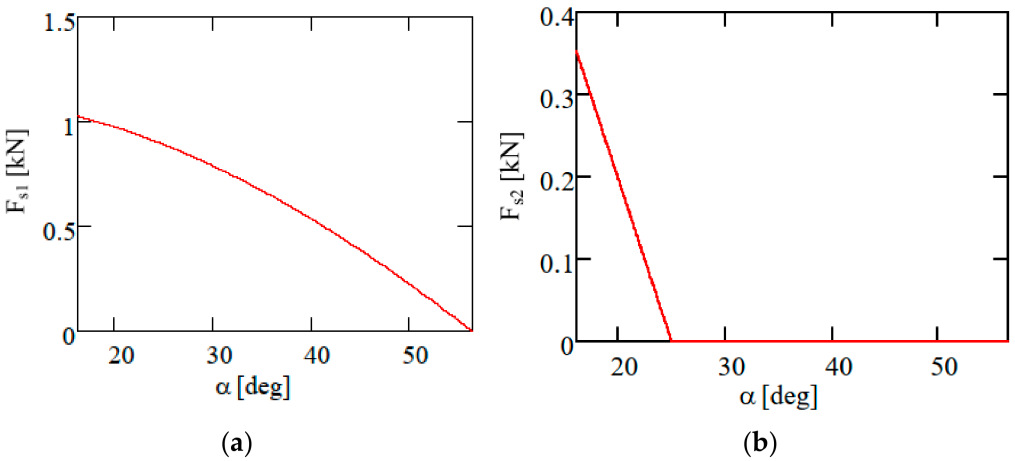


Figure 4. Dependences of the spring restoring forces on the arm inclination angle: (**a**) upper spring; (**b**) lower spring.

The derived analytical expressions were used to construct the force characteristics of the mechanism as functions of the arm inclination angle α for two cases: without springs and with springs taken into account, as shown in Figure 5.

The use of springs as a passive load compensation system has a positive effect on reducing the internal forces and the required driving force F_r (Table 1). However, the springs do not affect the vertical components of the reactions at the supports Y_a and Y_d and the pin joint Y_o.

The calculation results indicate that the use of the upper and lower springs reduces the required driving force by 26.5% and the internal forces by 19.8–39.6%.

The ratio of the required driving force F_r to the total weight G is given by

$$\frac{F_r}{G} = \frac{3.82}{1.5} = 2.55. \quad (7)$$

Table 1. Values of the support reactions, pin-joint reaction, and driving force.

Force Designation	Forces Values for $\alpha_{min} \ldots \alpha_{max}$, kN		Max-Value Percentage Difference, %
	No Springs	with Springs	
X_o	5.2 . . . 1.0	3.14 . . . 1.0	39.6
Y_o	0	0	0
Y_a	0.75	0.75	0
X_d	5.2 . . . 1.0	4.17 . . . 1.0	19.8
Y_d	0.75	0.75	0
F_r	5.2 . . . 1.0	3.82 . . . 1.0	26.5

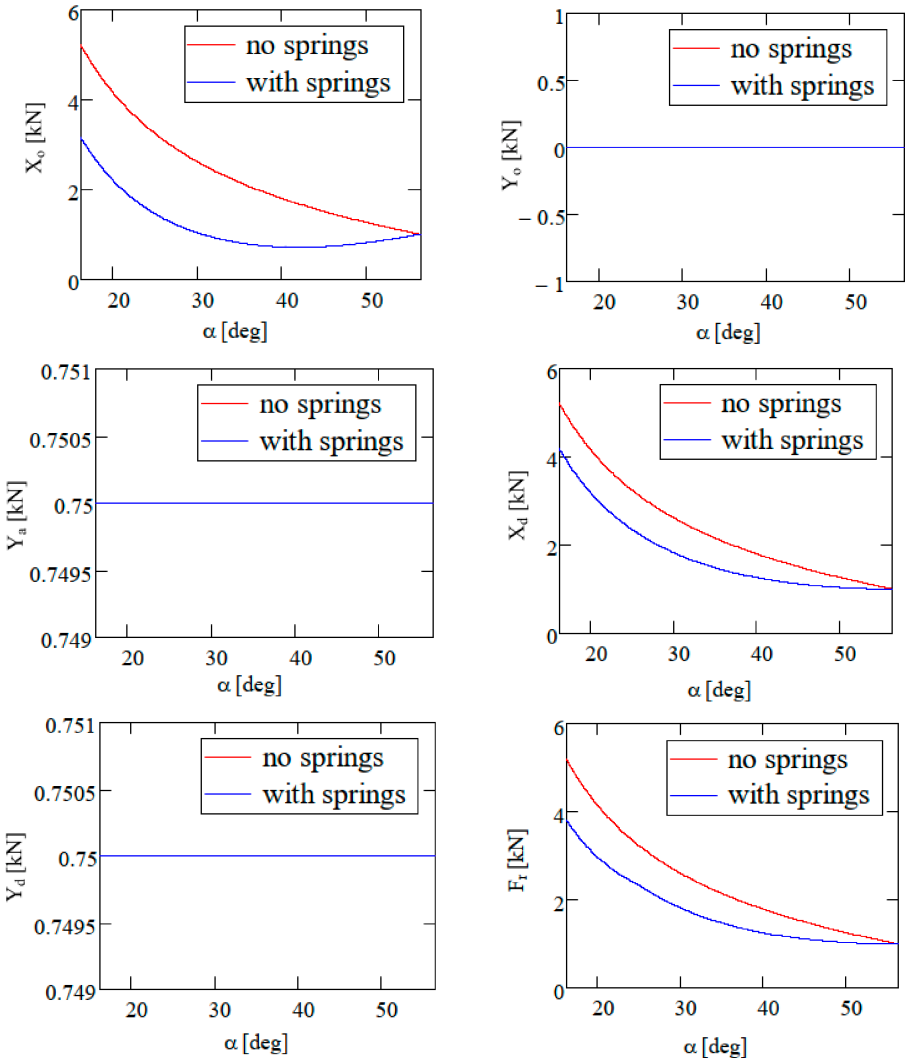


Figure 5. Dependences of the forces on the arm inclination angle.

6. Drive Power Calculation

To generate the required linear driving force, the drive system consists of a DC motor (1), a flexible coupling (2), gear transmissions (3), a ball screw (4), and a ball nut (5), which together convert rotary motion into the linear motion of the roller (6) (Figure 6).

https://doi.org/10.3390/engproc2026145010

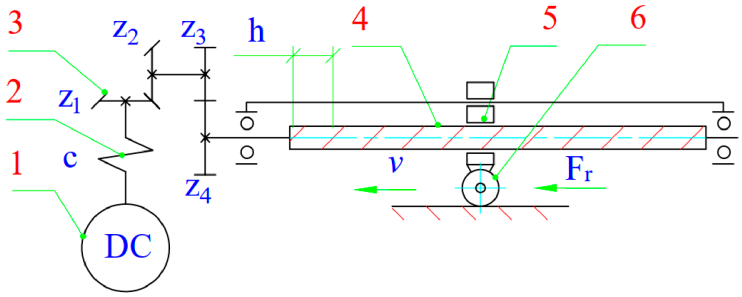


Figure 6. Kinematic scheme of the scissor lift drive: 1—DC motor; 2—flexible coupling; 3—gears; 4—ball screw; 5—ball nut; 6—roller.

The kinematic relationship between the motor and screw rotational speeds is given by

$$n_{DC}\frac{z_1}{z_2}\frac{z_3}{z_4} = n_{screw},$$

where n_{DC} is the rotational speed of the DC motor, n_{screw} is the rotational speed of the ball screw, and z_1, z_2, z_3, z_4 are the numbers of teeth on the corresponding gears.

For $n_{DC} = 3000$ rpm, $z_1 = z_2 = 28$, $z_3 = 16$ and $z_4 = 68$, the screw rotational speed is obtained as $n_{screw} = 0.235 n_{DC} = 0.235 \cdot 3000 = 705$ rpm.

The linear speed of the ball nut is determined as

$$v = \frac{\omega_{screw} h}{2\pi},$$

where h is the screw lead (h = 10 mm). Therefore, the linear speed of the ball nut is calculated as $v = \frac{0.235 \cdot 314 \cdot 10 \cdot 10^{-3}}{2\pi} = 0.118$ m/s.

According to Equation (4), the average platform lifting speed is $v_H = 1.36 \cdot 0.118 = 0.16$ m/s.

Alternatively, if the ball nut travel time is $t_2 = \frac{x_2}{v} = \frac{293.3}{118} = 2.48$ s, the platform lifting speed is $v_H = \frac{H}{t_2} = \frac{0.4}{2.48} = 0.16$ m/s.

The required motor power is calculated as

$$P_{DC} = \frac{P_{screw}}{\eta},$$

where P_{screw} is the power transmitted through the ball screw mechanism, $P_{screw} = F_r v$; η is the overall drive efficiency, $\eta = \eta_1 \eta_2 \eta_3$; η_1, η_2, η_3 are the efficiencies of the bevel gear transmission, spur gear transmission, and ball screw mechanism, respectively, $\eta = 0.98 \cdot 0.95 \cdot 0.85 = 0.79$.

Thus, the required motor power is calculated as

$$P_{DC} = \frac{3.82 \cdot 0.118 \cdot 10^3}{0.79} = 570 \text{ W}.$$

This calculation does not account for friction losses in the joints. According to the literature [10], the calculated power should be increased by 25–30% to compensate for these losses.

7. Conclusions

1. The scissor lift design incorporates upper extension springs and lower compression springs to reduce the required driving force transmitted through the ball screw drive. The stiffness coefficients of springs were determined, and their operating conditions were taken into account. In the lower position of the scissor lift mechanism, the upper

springs are fully extended and therefore generate their maximum restoring forces. As the platform is lifted, the restoring forces gradually decrease and become zero when the platform reaches its upper position. Conversely, the lower springs are fully compressed when the platform is in its lower position and extend during platform lifting until the scissor arm inclination angle reaches $\alpha = 25^\circ$.

2. The incorporation of the springs reduces the required driving force by 26.5% and the internal forces by 19.8–39.6% compared with the configuration without springs. For a required platform vertical travel of 400 mm, the corresponding horizontal travel of the ball nut is 293.3 mm. To achieve an average platform lifting speed of 0.16 m/s, the required motor power is 570 W. The obtained results demonstrate that incorporating upper and lower springs into the scissor lift mechanism is an effective approach to reducing the driving force and the support and joint reactions.
3. At this stage, the main kinematic and force characteristics were obtained based on the developed static model, confirming the feasibility of using additional compensation springs. The obtained results will serve as the basis for the synthesis, parameterization, and optimization of the drive arrangement of the developed scissor lift using the approaches proposed in [11–13]. During the parameter synthesis stage, the specific stiffness coefficients of the springs c_1 and c_2, together with their geometric parameters, will be determined based on the required load capacity G and platform lifting height H. In addition, the dynamic analysis of the system, accounting for the electromechanical processes in the drive and the nonlinear behavior of the ball screw drive, will be performed using the approach presented in [14].

Author Contributions: Conceptualization, V.G. and N.M.; methodology, V.G.; software, N.M.; validation, N.M. and V.B.; formal analysis, V.G. and N.M.; investigation, V.B.; resources, V.G. and N.M.; data curation, N.M.; writing—original draft preparation, V.G.; writing—review and editing, N.M.; visualization, N.M.; supervision, V.G.; project administration, V.G.; funding acquisition, V.B. All authors have read and agreed to the published version of the manuscript.

Funding: This research received no external funding.

Data Availability Statement: The raw data supporting the discussion and conclusions of this article will be made available by the authors on request.

Conflicts of Interest: The authors declare no conflicts of interest.

References

1. Korendiy, V.; Kachur, O. Locomotion Characteristics of a Wheeled Vibration-Driven Robot with an Enhanced Pantograph-Type Suspension. *Front. Robot. AI* **2023**, *10*, 1239137. [CrossRef] [PubMed]
2. Korendiy, V.; Krot, P.; Kachur, O.; Gurskyi, V. Analyzing the Locomotion Conditions of a Wheeled Vibration-Driven System with a V-Shaped Suspension. In *Advances in Design, Simulation and Manufacturing VII (DSMIE 2024)*; Lecture Notes in Mechanical Engineering; Springer: Cham, Switzerland, 2024; pp. 153–163.
3. Corrado, A.; Polini, W.; Canale, L.; Cavaliere, C. To Design a Belt Drive Scissor Lifting Table. *Int. J. Eng. Technol.* **2016**, *8*, 515–525.
4. Žiga, A.; Mešeljević, L.; Talić-Čikmiš, A. Static and Kinematic Analysis of the Scissor Lift STEM Toy. *Polytechnica* **2025**, *9*, 17–23. [CrossRef]
5. Dengiz, C.G.; Şenel, M.C.; Yıldızlı, K.; Koç, E. Design and Analysis of Scissor Lifting System by Using Finite Elements Method. *Univers. J. Mater. Sci.* **2018**, *6*, 58–63. [CrossRef]
6. Wozniak, M.; Morawski, J.; Zakrzewski, S.; Kądziela, A.; Szydłowski, T.; Siczek, K.; Szufa, S. Study on the Resistance to Friction in a Lead Screw-Nut Contact Zone in a Car Scissor Lift. *Adv. Sci. Technol. Res. J.* **2026**, *20*, 78–93. [CrossRef] [PubMed]
7. Wang, Y.; Guan, Y.; Hou, P.; Zhang, P.; Chen, Z. Development of a Horizontally Driven Multistage Scissor Lift Platform. In *Proceedings of the Sixth International Conference on Mechanical Engineering, Intelligent Manufacturing, and Mechatronics (MEIMM 2025), Guilin, China, 27–29 June 2025*; SPIE: Bellingham, WA, USA, 2025; Volume 13809, p. 138090E.
8. Gurskyi, V.; Kuzo, V.; Maherus, N.; Krot, P. Kinematic and Force Analysis of a Scissor Lift Mechanism. *Math. Models Eng.* **2025**, *11*, 230–242. [CrossRef]

9. Bembenek, M.; Nurkusheva, S.; Mykhailiuk, V.; Deineha, R.; Slabyi, O.; Kowalski, Ł.; Osyra, M. Lightweight Design and Safety Optimization of Scissor Lift Components Using FEM. *Syst. Saf. Hum.-Tech. Facil.-Environ.* **2026**, *8*, 58–69. [CrossRef]
10. Bulik, Y.; Pavliuk, V.; Tolstushko, M.; Tolstushko, N. Influence of Friction in Joints on Force Characteristics of Scissor Rolling Bridge Jack. In *Proceedings of the 25th International Scientific Conference Engineering for Rural Development, Jelgava, Latvia, 27–29 May 2026*; Latvia University of Life Sciences and Technologies: Jelgava, Latvia, 2026; pp. 1082–1088.
11. Dang, A.-T.; Nguyen, T.T.N. Investigation on the Design of Double-Stage Scissor Lifts Based on Parametric Dimension Technique. *Machines* **2023**, *11*, 684. [CrossRef]
12. Paramasivam, V.; Tilahun, S.; Jembere, A.K.; Selvaraj, S.K. Analytical Investigation of Hydraulic Scissor Lift for Modular Industrial Plants in Ethiopia. *Mater. Today Proc.* **2021**, *46*, 7596–7601. [CrossRef]
13. Dang, A.-T.; Nguyen, D.-V.; Nguyen, D.-N. Applying Parametric Analysis in Enhancing Performance for Double-Layer Scissor Lifts. *Stroj. Vestn.* **2023**, *69*, 299–307. [CrossRef]
14. Gurskyi, V.; Krot, P.; Maherus, N.; Dyshev, O. Nonlinear Dynamics Analysis and Design Optimization of an Electromechanical Actuator with Ball Screw Transmission. *Appl. Sci.* **2026**, *16*, 5200. [CrossRef]

Disclaimer/Publisher's Note: The statements, opinions and data contained in all publications are solely those of the individual author(s) and contributor(s) and not of MDPI and/or the editor(s). MDPI and/or the editor(s) disclaim responsibility for any injury to people or property resulting from any ideas, methods, instructions or products referred to in the content.